

Water Resources Research

RESEARCH ARTICLE

10.1002/2014WR016729

Key Points:

- A geostatistical approach to downscaling climate model data is presented
- Downscaled precipitation and temperature reproduce properties of the reference
- A variety of statistical indicators confirm the good performance of the method

Correspondence to:

S. K. Jha,
jha.sanj@gmail.com

Citation:

Jha, S. K., G. Mariethoz, J. Evans, M. F. McCabe, and A. Sharma (2015), A space and time scale-dependent nonlinear geostatistical approach for downscaling daily precipitation and temperature, *Water Resour. Res.*, 51, doi:10.1002/2014WR016729.

Received 27 NOV 2014

Accepted 11 JUL 2015

Accepted article online 21 JUL 2015

A space and time scale-dependent nonlinear geostatistical approach for downscaling daily precipitation and temperature

Sanjeev Kumar Jha^{1,2}, Gregoire Mariethoz^{1,3}, Jason Evans⁴, Matthew F. McCabe⁵, and Ashish Sharma¹

¹School of Civil and Environmental Engineering, University of New South Wales, Sydney, New South Wales, Australia,

²Extended Hydrological Prediction Section, Bureau of Meteorology, Canberra, Australian Capital Territory, Australia,

³Institute of Earth Surface Dynamics, University of Lausanne, Lausanne, Switzerland, ⁴Climate Change Research Center, University of New South Wales, Sydney, New South Wales, Australia, ⁵Division of Biological and Environmental Sciences and Engineering, King Abdullah University of Science and Technology, Thuwal, Saudi Arabia

Abstract A geostatistical framework is proposed to downscale daily precipitation and temperature. The methodology is based on multiple-point geostatistics (MPS), where a multivariate training image is used to represent the spatial relationship between daily precipitation and daily temperature over several years.

Here the training image consists of daily rainfall and temperature outputs from the Weather Research and Forecasting (WRF) model at 50 and 10 km resolution for a 20 year period ranging from 1985 to 2004. The data are used to predict downscaled climate variables for the year 2005. The result, for each downscaled pixel, is daily time series of precipitation and temperature that are spatially dependent. Comparison of predicted precipitation and temperature against a reference data set indicates that both the seasonal average climate response together with the temporal variability are well reproduced. The explicit inclusion of time dependence is explored by considering the climate properties of the previous day as an additional variable. Comparison of simulations with and without inclusion of time dependence shows that the temporal dependence only slightly improves the daily prediction because the temporal variability is already well represented in the conditioning data. Overall, the study shows that the multiple-point geostatistics approach is an efficient tool to be used for statistical downscaling to obtain local-scale estimates of precipitation and temperature from General Circulation Models.

1. Introduction

Accurate prediction of precipitation and temperature is critical for many hydrological, ecological, and environmental studies. Indeed, considerable effort has been expended on characterizing the future behavior of hydrological and related systems, particularly in response to potential changes in the climate system. Unfortunately, the output from General Circulation Models (GCMs) is generally too spatially coarse to be used directly in impact assessment of climate change at the regional level [Almazroui, 2012]. In such applications, downscaling techniques need to be applied in order to impart small-scale variability to the GCM outputs. Dynamical downscaling (physics based) and statistical downscaling (data driven) represent the two broad categories of downscaling techniques that are routinely employed.

In dynamical downscaling, a Regional Climate Model (RCM) is applied to incorporate detailed terrain and land cover information, using GCM outputs and observations to define initial and boundary conditions [McGregor, 1997; Meng *et al.*, 2014]. Although computationally expensive, dynamical downscaling produces fine-resolution data over a limited region of interest. In statistical downscaling, empirical relationships are developed between coarse-scale climate variables and those at a finer scale [Fowler *et al.*, 2007]. The approach is computationally fast and can downscale the data in both space and time. The selection of predictors is based on their availability in the GCM outputs. An empirical relationship between predictors and predictands is assumed to hold true under future climatic scenarios. Typically, statistical downscaling approaches are applied to each variable of interest independently with no consideration of the physical connections between variables. All of these assumptions have been debated due to the nonlinear nature of atmospheric processes.

Geostatistics represent a natural tool to apply when modeling spatially correlated variables. The success of geostatistical simulations in geology, earth science, and remote sensing are well recognized [Atkinson *et al.*, 2008; Ge and Bai, 2010; Mariethoz *et al.*, 2012; Zhang *et al.*, 2012]. However, the applications of geostatistics in climate model downscaling of precipitation and temperature are relatively few. Biau *et al.* [1999] used kriging to build a statistical model between coarse-scale climate variables and local variables. Fiorucci *et al.* [2001] applied linear geostatistics to reconstruct rain field at finer scale using large-scale information as conditioning data. Conditioning data can be understood as the known data set that the simulation algorithm will respect while producing results. However, the use of variogram-based geostatistics does not account for the known complexity of precipitation fields [Lanza *et al.*, 2001]. For instance, temperature is strongly related to precipitation, as the moisture holding capacity of the atmosphere is linked to air temperature. In the case of multiple climate variables, methods relying on assumptions of linearity and multi-Gaussianity will not be sufficient and novel approaches are needed.

Multiple-point geostatistics (MPS) is a family of nonparametric algorithms that use training images to derive spatial arrangements of values. MPS was originally developed for modeling geological features that present strong contacts and connected structures. These are properties that variogram often fails to represent accurately [Emery and Lantuéjoul, 2014; Journel and Zhang, 2006; Mariethoz *et al.*, 2010; Neuweiler *et al.*, 2011; Zinn and Harvey, 2003]. Although traditionally applied to subsurface modeling problems [Caers and Zhang, 2005; Strebelle, 2002], MPS has been increasingly used for surface hydrology [Boucher *et al.*, 2008], remote sensing applications [Ge and Bai, 2011; Mariethoz *et al.*, 2012], and to represent climatic variables either as time series [Oriani *et al.*, 2014] or in a spatially distributed context using only categorical variables [Wojcik *et al.*, 2009]. Jha *et al.* [2013b] pioneered the use of MPS for climate model downscaling by developing an application to downscale seasonal maps of latent heat flux, surface temperature, and soil moisture. The results provide physically consistent spatial patterns of land-atmosphere variables, with the nonlinear relationships between the variables preserved in the MPS simulation. The main advantage of MPS over multi-Gaussian kriging-based approaches is its ability to capture and reproduce local spatial structures. The combination of a traditional geostatistical approach (area to point cokriging) with MPS was applied by Tang *et al.* [2015] to integrate satellite images at coarse and finer resolution obtained from different sources and thus obtain desired fine-resolution image. Area to point cokriging was required to take into account the change of support of spatial features at different scales. The resulting image was used as conditioned data for the MPS simulation.

The goal of this study is to develop a geostatistical approach based on MPS to downscale precipitation and temperature. We base the model development on our previous work presented in Jha *et al.* [2013b]. The extension of the previous approach to the present study is not trivial due to number of reasons:

1. In Jha *et al.* [2013b], we used seasonal mean values of 20 years of information on soil moisture, latent heat flux, and surface temperature. So the time dimension was implicitly considered. In this work, we use daily precipitation and temperature record of past 20 years to build the training image. In the training image, we are not only considering spatial information but also temporal information. Additionally, in the present study, we test the importance of including temporal dependence by considering two scenarios with and without time dependence (discussed in section 2.4 below).
2. It is a known fact that the precipitation is much more difficult to simulate than land-atmospheric variables like soil moisture, latent heat flux, etc. Precipitation has a much more complex spatial structure and behavior than other climatic parameters because the generation of precipitation involves nonlinear and sensitive physical processes [Bardossy and Plate, 1992]. Several stochastic approaches such as autoregressive and Markov-chain-based models [Mehrotra and Sharma, 2007] and recently MPS [Oriani *et al.*, 2014; Wojcik *et al.*, 2009] have been applied to model both occurrence and amount of precipitation. Due to its non-Gaussian nature, its skewed distribution, its binary-type response (with either presence or absence of rainfall), and the necessity of capturing both the mean and extreme values in the downscaled information, downscaling precipitation is more challenging than other land-atmosphere variables [Vrac and Naveau, 2007]. Most of the downscaling efforts produce better temperature than precipitation estimates because of difficulty in capturing the daily precipitation amounts and spatial and temporal patterns correctly [Maraun *et al.*, 2010]. Even at the cost of expensive computation, the regional climate models often produces precipitation which occur too frequently and with low average intensity [Dai *et al.*, 2004; Iorio *et al.*, 2004; Sun *et al.*, 2006]. The statistical downscaling approaches are constrained by the availability of length of the GCM output. The variance of the downscaled precipitation is often lower than the variability

in observed data [von Storch, 1999]. It is also broadly recognized that maintaining spatial dependence in the downscaled precipitation time series at multiple sites is challenging and therefore hybrid downscaling methods have been developed [Alaya *et al.*, 2015; Jiang and Yang, 2012].

In this work, a multivariate, multiple-point geostatistical approach is developed which takes into account space-time dependence of precipitation and temperature, therefore producing for each downscaled pixel, a daily precipitation and temperature time series, where each value is also spatially dependent on its neighbors. Both spatial and temporal dependence are inferred from historical data sets that are used to create the training images.

2. Methodology

Following is a brief overview of the Direct Sampling and MPS approach, as well as a description of the study site and the development of training images and conditioning data. Further details on this approach and methodology can be found in Mariethoz *et al.* [2010] and Jha *et al.* [2013b].

2.1. Training Data

MPS algorithms require a training image and a simulation grid. The procedure then generates one or several random variables (Z_1, \dots, Z_k) on the simulation grid, by deriving spatial statistics from the training image, which contains the features expected in the modeled spatial phenomena. Depending upon the nature of the study, the structure of the training image could be two-dimensional (2-D) or three-dimensional (3-D). For example, a 2-D training image is sufficient to characterize the bed forms in a large river [Jha *et al.*, 2013a], while for geological modeling of an alluvial aquifer, a 3-D training image may be necessary [Comunian *et al.*, 2014; Jha *et al.*, 2014]. The success of MPS relies on the selection of an appropriate training image. In the present study, this consists of 2-D images of daily precipitation and temperature at both coarse and fine resolution. Considering that the precipitation on any particular day may be related probabilistically to precipitation on the previous day, the training image could also include that information. In other applications, the training image may be nonstationary, demanding that such variables be described using auxiliary information such as distance from coast or vegetation, thereby enhancing the identification of regions with similar patterns [Honarkhah and Caers, 2012]. In the present study, the temporal stacking of 2-D images of daily rainfall images effectively results in a 3-D space-time training image. Further addition of several variables leads to a multivariate training image, which are also developed throughout this analysis.

2.2. Direct Sampling Algorithm

Among several possible MPS algorithms, the Direct Sampling (DS) is used in this particular application because the method allows for using a multivariate training image, which is needed to characterize the relationship between multiple climatic variables. Details of the DS algorithm can be found in Mariethoz *et al.* [2010] and practical guidelines on the selection of appropriate parameter values can be found in Meerschman *et al.* [2013]. In essence, the algorithm populates a regular grid with patterns derived from the training image, conditioned to known values for certain locations and time stamps and termed conditioning data. Each grid pixel \mathbf{x} is visited sequentially according to a random path (here \mathbf{x} denotes a location in 3-D space, comprising 2-D space and time). To determine the value at \mathbf{x} , denoted $Z(\mathbf{x})$, the pattern (or neighborhood) surrounding \mathbf{x} , denoted $\mathbf{N}_x = [Z(\mathbf{x} + \mathbf{h}_1), \dots, Z(\mathbf{x} + \mathbf{h}_n)]$. The neighborhood of a pixel \mathbf{x} is defined as the n closest informed pixels to \mathbf{x} separated by a vector \mathbf{h} . A similar pattern is then sought in the training image, denoted $\mathbf{N}_y = [Z(\mathbf{y} + \mathbf{h}_1), \dots, Z(\mathbf{y} + \mathbf{h}_n)]$, and the training image value $Z(\mathbf{y})$ at the corresponding location \mathbf{y} in the training image is then pasted at the simulated location \mathbf{x} . In case of multiple variables, the neighborhood is defined for each of the m variables as $\mathbf{N}_x^k = [Z_k(\mathbf{x} + \mathbf{h}_{1,k}), \dots, Z_k(\mathbf{x} + \mathbf{h}_{n,k})]$, where $k = 1, \dots, m$. The joint neighborhood through all the variables can be estimated as the ensemble of all the individual neighbors as $\mathbf{N}_x^k = [\mathbf{N}_x^1, \dots, \mathbf{N}_x^m]$. Similarly, a pattern \mathbf{N}_y^k can be estimated in the multivariate training image.

The similarity between both patterns \mathbf{N}_x^k and \mathbf{N}_y^k is established using a distance function $d(\mathbf{N}_x^k, \mathbf{N}_y^k)$. Mariethoz *et al.* [2010] proposed number of possible distance functions for the categorical and continuous variables, such as the weighted Euclidean distance. In this study, a normalized Manhattan distance is computed for each variable k as

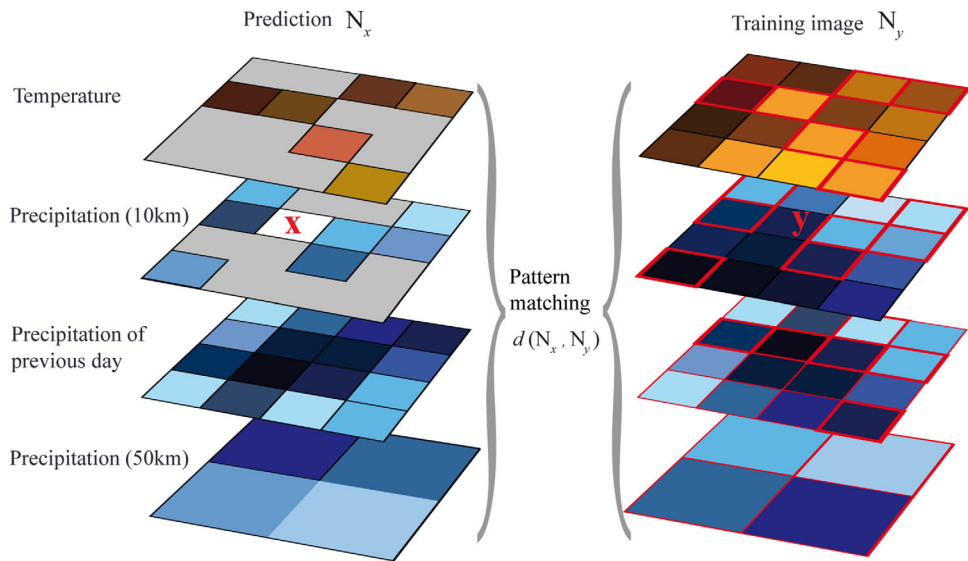


Figure 1. Illustration of the pattern matching procedure used in direct sampling with multiple variables at coarse and fine resolutions. The layers on the right indicate information contained in the training data, while the layers on the left indicate the simulation grids with conditioning data.

$$d(\mathbf{N}_x^k, \mathbf{N}_y^k) = \frac{1}{n} \sum_{i=1}^n \frac{|Z^k(\mathbf{x}_i) - Z^k(\mathbf{y}_i)|}{\max_{y \in Tl} Z^k(y) - \min_{y \in Tl} Z^k(y)} \in [0, 1] \quad (1)$$

where n is the number of nodes in the pattern considered. n is chosen for each variable such that the number of neighbors reflects the complexity of the patterns present in this variable.

In the case of multiple variables, the algorithm is extended by defining the random path through all variables, using their neighborhoods and computing a multivariate distance that is a linear combination of several univariate distances.

$$d(\mathbf{N}_x, \mathbf{N}_y) = \sum_{k=1}^m w_k d(\mathbf{N}_x^k, \mathbf{N}_y^k) \quad (2)$$

where m is the number of variables, w_k is the weight of each variable k , and $\sum_{k=1}^m w_k = 1$.

The multivariate feature of the DS algorithm is very important in this study because the information at different spatial resolutions and also from previous days (time dimension) is represented as additional variables. In the case of rainfall simulation, information from the previous day may be important, but not as important as that of the current day. As it is clear from equation (2), the degree of influence of each variable on the simulated field depends on the weights w_k , which allow explicit accounting of the different degrees of influence that each variable has on the simulation result. Another feature specific to geostatistical methods is the ability to produce multiple random realizations of the downscaled field. This allows for the derivation of a local probability distribution for each downscaled pixel, which can be used for assessing the uncertainty inherent to the downscaling procedure.

Figure 1 describes a possible setup for the training image and conditioning data. Since we are dealing with training images that are relatively complex objects, we will use the term training data in the following discussion. In Figure 1, \mathbf{x} refers to a position in the simulation grid (left-hand side) where a prediction is needed and \mathbf{y} refers to a position in the training data (right-hand side) where all variables are informed. The stacked layers represent the different variable in the training data set. In this specific case, four variables (precipitation and temperature at 50 and 10 km resolutions) are modeled, with a pair of variables representing coarse and fine-scale information for the property being downscaled, which in this case is precipitation. In the training data, all variables are fully informed at both 50 and 10 km resolutions, and for 20 years at a daily time step. In the simulation grid (where a downscaled prediction is needed), only the coarse 50 km resolution and the fine resolution of the previous

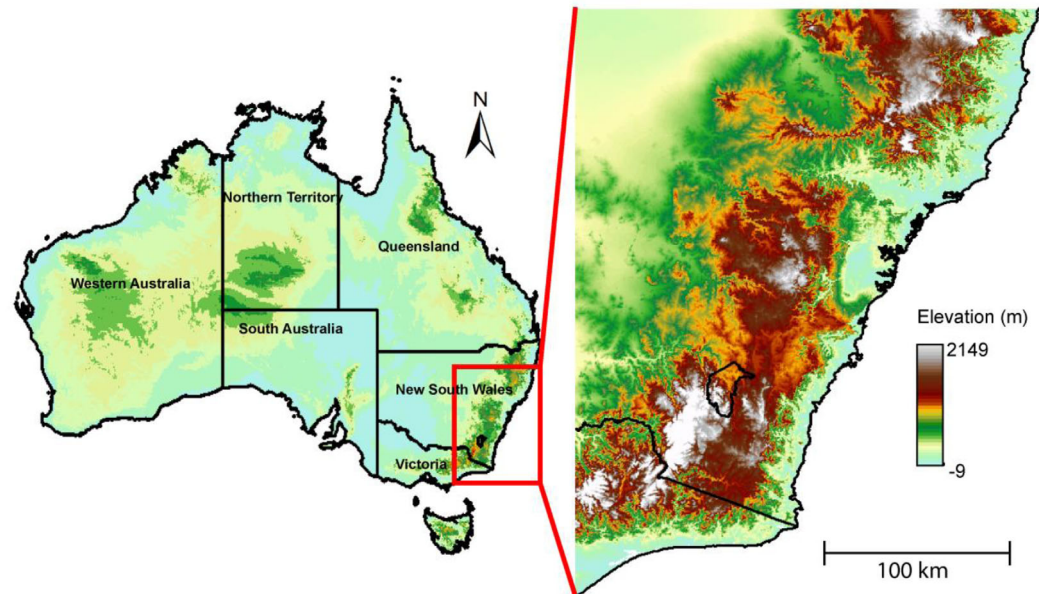


Figure 2. Study area in south-eastern Australia.

day (previously downscaled) are known. Direct Sampling is used to populate precipitation and temperature at the fine 10 km scale, using values that correspond statistically to the patterns found in the coarser resolution training data set. Here the conditioning data contain information only at the 50 km resolution as well as information from the previous day. Note that Figure 1 represents a specific setting with four variables, but in practice more variables can be considered, including coarse temperature or locational variables such as latitude, longitude, and elevation which help in describing nonstationary properties of the modeled domain. In the following sections, we will present applications involving up to nine variables.

2.3. Study Domain and Data

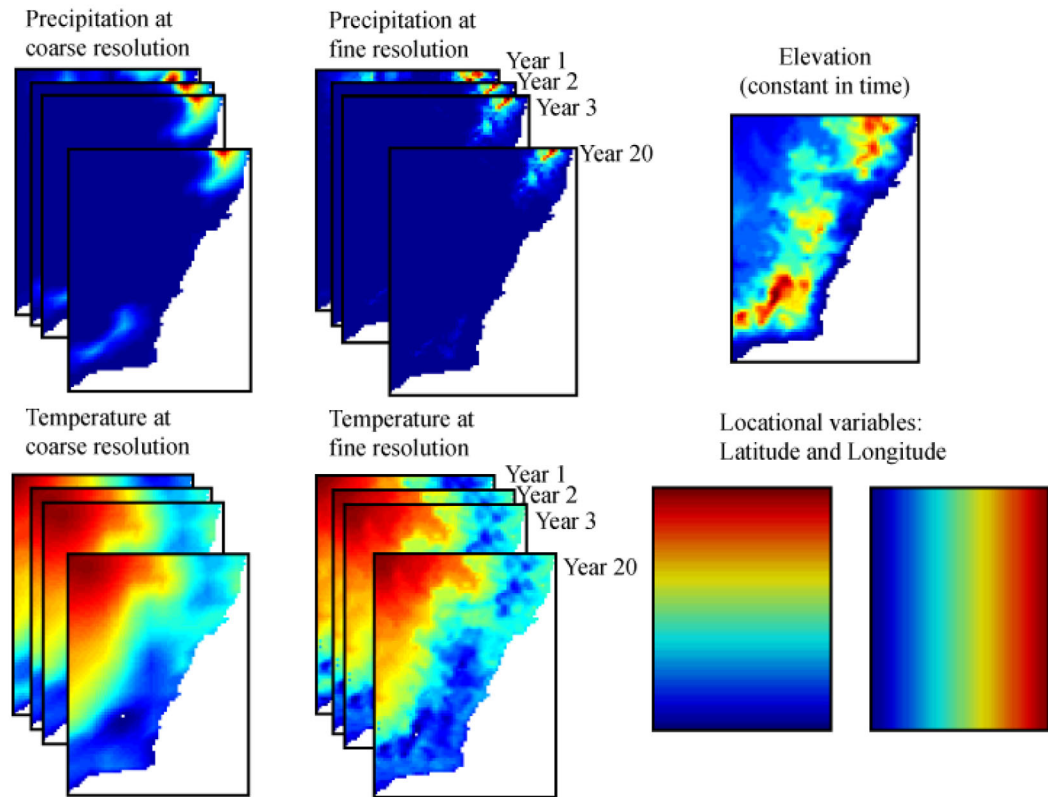
The study area is located in south-eastern Australia, spanning longitudes 147°E–154°E and latitudes 30°S–39°S as shown in Figure 2. It encompasses part of the Murray-Darling basin, which is the largest and most economically productive catchment in Australia and where further understanding of the impact of climate change on long-term productivity and sustainability is required. There are two main reasons for choosing this site: (1) the results from the WRF model at spatial resolution of 50 km (coarse resolution) and 10 km (fine resolution) are available from the work of *Evans and McCabe [2010]*, and (2) the geographical conditions of the study area include coastal to inland areas, with both lowlands and mountains that create large gradients in climatic variables over a relatively short distance. Orographic effects due to mountains and the temperature variation due to proximity with the ocean create high and low-pressure zones, causing occasional heavy rains near coastal regions. The study area has dynamic weather patterns and mesoscale influences, which make it challenging to develop a downscaling approach for precipitation and temperature.

Twenty years (1985–2004) of daily precipitation and daily temperature at both 50 and 10 km were extracted from the WRF output to construct the training data set. The chosen model domain has dimensions of 71 by 91 grid cells, with a cell size of 10 km. For the year 2005, it is assumed that information is available only at 50 km resolution, which is used as conditioning data. The direct sampling approach is then applied to obtain predictions of rainfall and temperature at 10 km resolution for the year 2005, and the results are used for evaluating the downscaling methodology.

2.4. Development of Training Images and Conditioning Data

In this study, two scenarios are considered. In the first scenario (Scenario 1), which is illustrated in Figure 3, the temporal dependence of precipitation (P) and temperature (T) is explicitly modeled. The training

a) Training image (7 variables)



b) Conditioning data (same 7 variables)

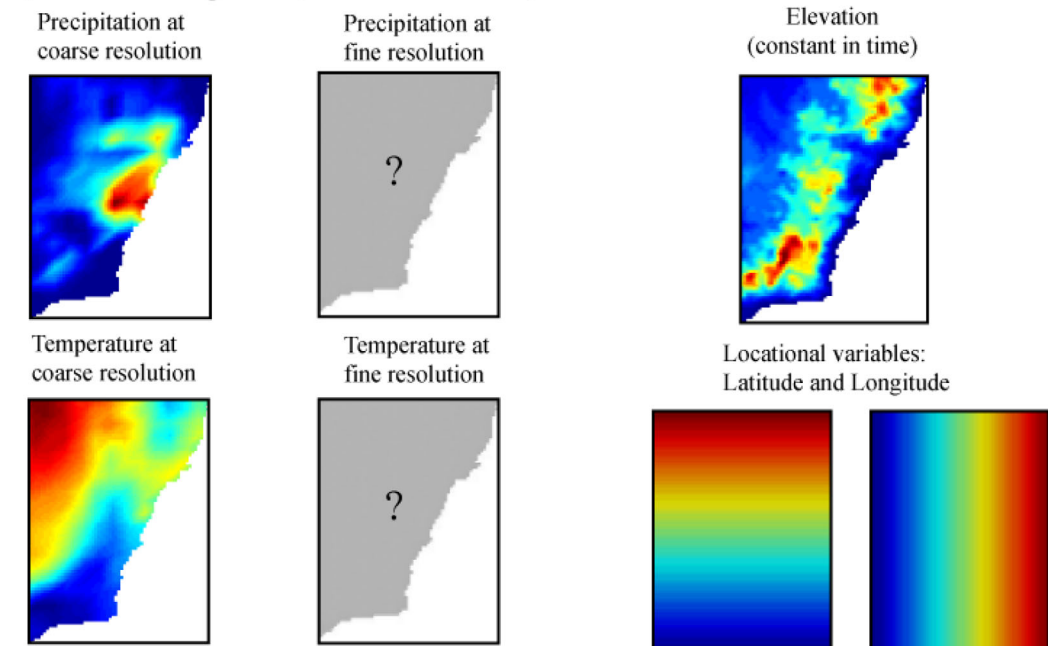


Figure 3. Schematic illustration of the model setting for Scenario 1 (ignoring time dependence). (a) Arrangement of available daily information in space and time at coarse and fine resolutions for years 1985–2004, used in the training data, and (b) available information at coarse resolution for a single day of year 2005, used as conditioning data to simulate precipitation and temperature on the simulation grid at the fine resolution.

Table 1. Parameters Used for the Direct Sampling Algorithm

Variables	Scenario 1 (Ignoring Time Dependence)		Scenario 2 (Considering Time Dependence)	
	n	w	n	w
t (distance threshold)	0.001		0.001	
f (fraction of training image scanned)	0.5		0.5	
Maximum search radius	20		20	
P_{50}	20	1	20	1
P_{10}	20	1	20	1
T_{50}	20	1	20	1
T_{10}	20	1	20	1
P_{50} previous	N/A	N/A	20	0.3
T_{50} previous	N/A	N/A	20	0.3
Latitude	1	0.01	1	0.01
Longitude	1	0.01	1	0.01
Z	1	0.1	1	0.1

data contains information on daily precipitation and daily temperature at both coarse 50 km and fine 10 km resolutions for 20 years (years 1985–2004). To address nonstationarity in the training image, locational variables (latitude, longitude, and elevation) are also included to restrain the sampling of patterns in the vicinity of the pixel being simulated. Hence, there are seven variables in this scenario: P_{50} , P_{10} , T_{50} , T_{10} , latitude, longitude, and elevation (the subscripts are used to differentiate between the 10 and 50 km resolutions for climatic variables; locational variables are all known at a 10 km resolution). In the simulation grid, the same seven variables are considered, but conditioning data only inform the variables that are known for year 2005, which include P_{50} , T_{50} , and the locational variables for any given day of that year.

In the second scenario (Scenario 2), the same seven variables are used, with the addition of climatic information from the previous day, WRF output at 50 km resolution. As a result, this scenario considers nine variables: the same variables as in the first scenario and additionally P_{50} and T_{50} of the previous day. This scenario explicitly accounts for the temporal dependence of these variables, as opposed to the first scenario that simulates each day independently of the previous one.

In both scenarios, P_{10} and T_{10} , which are the target of the downscaling procedure, are unknown in the simulation and are stochastically generated using the direct sampling algorithm by considering spatiotemporal patterns derived from the training data.

2.5. Parameterization of the Direct Sampling Approach

The parameters used in the direct sampling approach largely follow the guidelines provided in Meerschman *et al.* [2013] and are detailed in Table 1. In Scenario 1 (ignoring temporal dependence), the number of neighbors for each climatic variable is set to $n = 20$ pixels. A neighborhood of only 1 pixel is used for the locational variables, as it is sufficient to define the position of \mathbf{x} in order to describe nonstationary behavior.

An important parameter is the weights w_k given to each variable in the distance function. While these weights should in principle sum to one, it is easier in practice to use relative weights, which can then be normalized at a later stage to ensure that they sum to one. Hence, a constant relative weight of 1 is given to all climatic variables (P_{50} , P_{10} , T_{50} , and T_{10}). The locational variables are given lower weights of 0.01 for *Lat* and *Lon*, and 0.1 for *Z*. The weight of elevation is greater than that of latitude and longitude because the elevation is expected to have a stronger influence on climatic variables. These weights have been determined by carrying out a sensitivity analysis on a small subdomain that investigated variogram reproduction for a range of reasonable w_k values for the climatic and locational variables. The main finding, in line with the authors empirical experience, is that small weights given to the locational variables are sufficient to produce nonstationarity models. We acknowledge that the weights could be further optimized, for example, by increasing the w_k of the climatic variables that have a strong spatial dependence. However, at the present time, there is no unified methodology to quantitatively determine these weights, for example, with a specific cross-validation procedure. Therefore, the results presented thereafter can probably be improved if such a procedure can be developed in the future. In Scenario 2, which considers temporal dependence, T_{50}

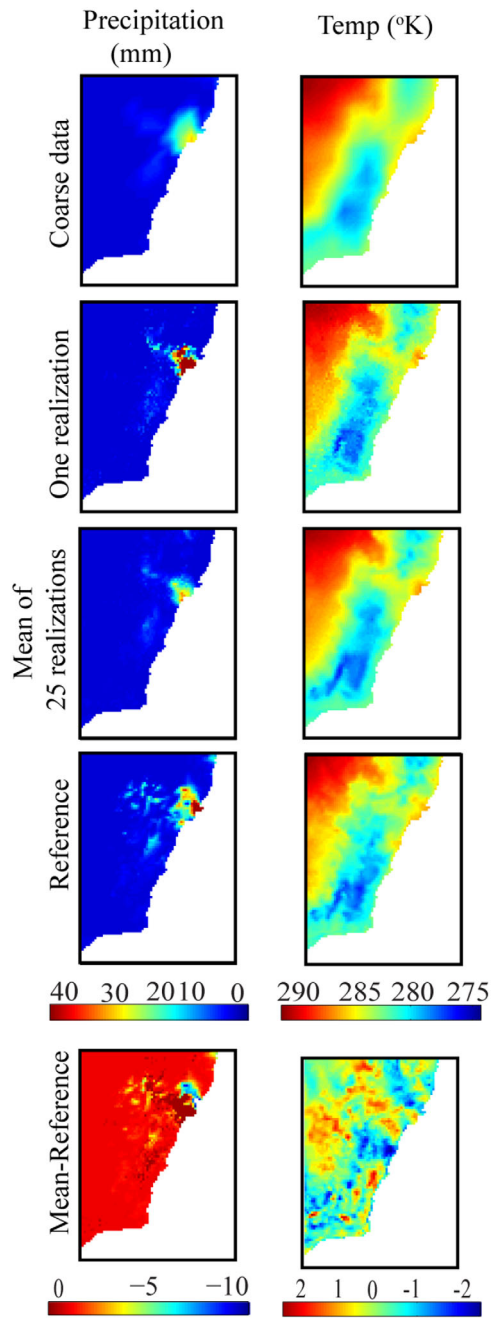


Figure 4. Downscaling results using the MPS approach for precipitation and temperature for DOY 101 of 2005. (first row) The coarse resolution (50 km) conditioning data, (second row) one randomly sampled downscaled realization (10 km) obtained via direct sampling. (third row) The mean values of 25 realizations. (fourth row) The reference (WRF retrieved reference simulation at 10 km). The difference between rows three and four is shown in fifth row.

of year 2005. Day 1 is not considered in the simulation to avoid providing information on the previous day (day 0, which does not exist) that is required in Scenario 2. The simulation for each day is run separately for 25 realizations, resulting in an ensemble of 25 different values at each point of the domain, which is used to assess the uncertainty in the downscaled values. To illustrate the results, Figure 4 presents the downscaling of P and T for day of year (DOY) 101 in Scenario 1. Any other day could have been used for demonstration

and P_{50} of the previous day are given a weight of 0.3, which corresponds to the value of the temporal lag-1 autocorrelation function of rainfall that is observed in the 20 years of training data, averaged over all locations in the study area. Other parameters described in Table 1 are not specific to each variable and are set according to the guidelines of Meerschman *et al.* [2013].

2.6. Statistical Measures

Several statistical measures are used in this study to evaluate the performance of the downscaled results. We estimate daily probability density functions (pdfs) for the downscaled results and compare these to daily pdfs obtained from the reference WRF data. In the calculation of pdfs, precipitation below 0.2 mm was classified as nonrainning.

Downscaling results are compared against the reference using the Perkins skill score [Perkins *et al.*, 2007] and bias plots. Perkins skill score (S_{score}) is the measure of the common area between daily pdfs of simulated and reference values defined as follows:

$$S_{score} = \sum_i^N [\min(P_i^{simulated}, P_i^{reference})] \quad (3)$$

where N is the number of bins used to calculate the pdfs. $P_i^{simulated}$ and $P_i^{reference}$ are frequencies of values in a given bin in the simulation and reference histograms. A Perkins skill score of 1 is achieved when the pdfs completely overlap and 0 occurs if they do not overlap at all.

In Australia, there is a considerable difference between the seasonal precipitation patterns throughout the year. As such, it is important to observe whether the MPS approach is able to capture the expected seasonality of precipitation and temperature patterns. To estimate a bias map for each day, the WRF-based reference (O) is subtracted from the ensemble average of the 25 realizations for each day (\bar{M}) as follows:

$$Bias = \bar{M} - O \quad (4)$$

3. Results

3.1. Evaluation of the Downscaled Results

The downscaling approach is applied to simulate daily precipitation and temperature for days 2–365

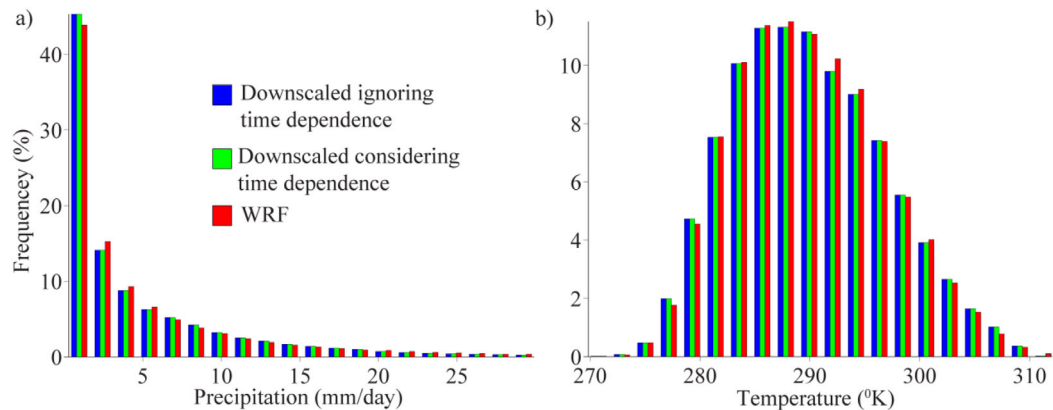


Figure 5. Probability density function (pdf) of daily (a) precipitation and (b) temperature. Precipitation less than 0.2 mm d^{-1} are disregarded in the estimation of pdf.

purpose but the day 101 is chosen because the zone of high precipitation is clearly visible on the eastern region in the plot (Figure 4). The idea is to demonstrate how MPS simulation could use training data and coarse-scale information to predict fine-scale features, and to compare these results with the known reference. The coarse resolution P_{50} and T_{50} in the first row of Figure 4 are provided as conditioning data. The second row shows a randomly sampled realization of the downsampled values (P_{10} and T_{10}), which is comparable to the reference values (WRF 10 km output) shown in the fourth row. The mean of 25 realizations is shown in third row and the difference between mean and reference in fifth row. As can be seen, the downscaling approach is able to reproduce realistic spatial patterns and features of P and T , similar to those observed in the reference data set. The downsampled precipitation map is slightly noisier than the reference, but the most important spatial features have been resolved. In particular, the rain cell present in the eastern portion of the domain is accurately positioned, whereas on the coarse data, it is present only as an area of diffuse rainfall. The temperature map also presents detailed features that are correctly identified, although as with the precipitation reproduction, the result is not as smooth as the reference. The difference between the mean value of 25 realizations and the reference (Figure 4, fifth row) shows that in most of the area, the error is close to zero apart from a few locations where the downsampled prediction has not been able to capture the peak values. The difference between mean prediction and reference shows large negative errors for rainfall in the north-eastern part of the domain, due to a small shift in the location of the maximum rainfall intensity. For temperature, the estimation errors are small throughout the domain.

3.2. Probability Density Functions

Figure 5 shows the pdfs of daily precipitation and daily temperature for the year 2005. In Figure 5a, only events with precipitation below 30 mm are shown, as the frequency of events with precipitation higher than 30 mm is low (1.38% of the pdfs), which is also evident in the time series plots (Figure 9) presented in the next section. Twenty bins are considered in generating histograms in Figure 5, which means each bin has a width of 1.5 mm d^{-1} on the x axis. The pdfs obtained from Scenarios 1 and 2 (ignoring or considering time dependence) were similar to those obtained from the reference.

The pdfs of daily temperature are shown in Figure 5b, and show that the downscaling results have a pdf that is very similar to the reference.

3.3. Skill Score

Plots of Perkins skill score for precipitation obtained from Scenarios 1 and 2 are shown in Figures 6a and 6b. Over large areas, the downscaling approach is able to correctly capture the daily pdf of precipitation with a mean Perkins skill score of over 0.8, with the coastal areas having higher skill scores than the inland. Conversely, areas on the western side of the model domain have relatively low skill scores. Figures 6c and 6d show plots of Perkins skill score of mean temperature, showing that the downscaling is more accurate than for precipitation, with an average skill score of 0.88.

By comparing the left and right columns of Figure 6, it can be seen that results from both Scenarios 1 and 2 are very similar. The average value of the skill score for precipitation is 0.80 for Scenarios 1 and 2, while for

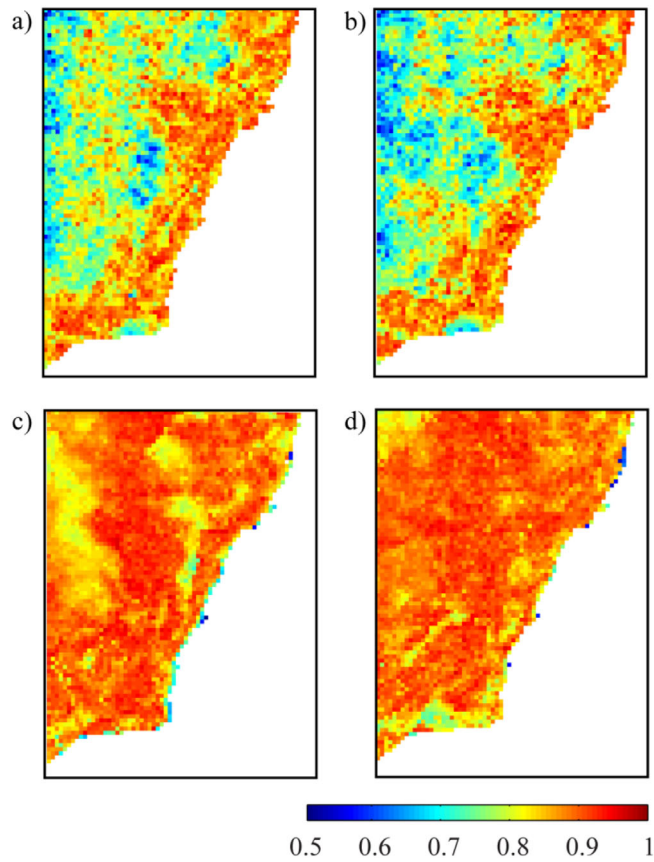


Figure 6. Perkins skill score across the domain for (top) daily precipitation and (bottom) daily temperature with Figures 6a and 6c corresponding to Scenario 1, while Figures 6b and 6d corresponding to Scenario 2.

temperature the average skill score is 0.88 in Scenarios 1 and 2. In considering the skill score alone, there seems to be little advantage in adding information from the previous day. As will be seen, this result does not hold true for other statistical measures of performance.

3.4. Seasonal Bias Plots

The bias plot of seasonal mean precipitation is shown in Figure 7, with the first and second rows corresponding to results obtained from Scenarios 1 and 2, respectively. Each column corresponds to the results for a season, defined as summer: December to February (DJF), autumn: March to May (MAM), winter: June to August (JJA), and spring: September to November (SON). Note that the seasons mentioned here correspond to Southern Hemisphere (austral) seasons.

The seasonal mean values of precipitation and temperature bias estimated over the entire study area in different seasons are listed in Table 2. Scenario 2 provides lower bias values than Scenario 1, indicating that the prediction improves across all seasons when including the previous day information. While the precipitation is underestimated for all seasons, especially in winter and spring, the magnitude of the bias values is relatively small, ranging between -1.034 and -0.14 mm d^{-1} for these seasons for year 2005.

Figure 8 presents the bias plots of seasonal mean temperature, with the same arrangement as in Figure 7. It is noted that the bias magnitudes are very small, and that there is no defined pattern observed in regionalization of high and low values of bias in temperature over the seasons. As for precipitation, conditioning the downscaled simulations on the previous day's information (Scenario 2) improves the prediction of down-scaled temperature.

3.5. Evaluation of the Temporal Behavior

In the previous section, we presented the performance of our approach in reproducing spatial patterns over the study area. While a summary of temporal aspects was implicitly included in the discussion on skill scores,

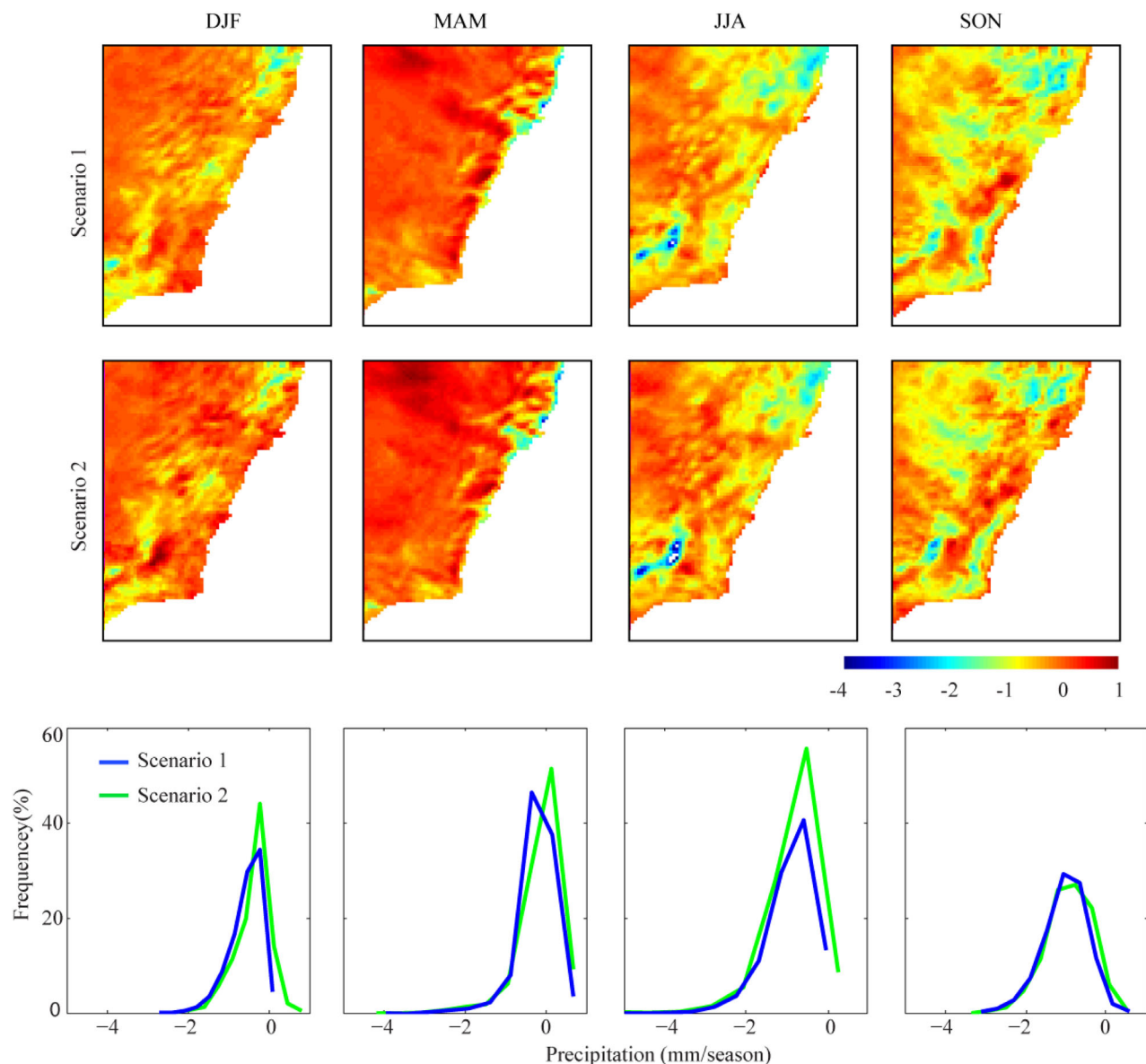


Figure 7. Comparison of seasonal mean precipitation bias plots obtained for (first row) Scenario 1 and (second row) Scenario 2. (third row) Corresponding pdfs. DJF, MAM, JJA, and SON define the seasons of summer, autumn, winter, and spring, respectively.

In this section, we more closely examine the performance of the MPS approach in reproducing temporal patterns. Figures 9 and 10 present a time series of precipitation and temperature at a grid point obtained from 25 realizations of DS simulations and compared with the reference for the same duration (days 2–365 of year 2005). Note that the approach produces 25 such time series ensembles for each pixel of the model grid. Each green line in Figure 9a or blue line in Figure 9b corresponds to one downscaling realization. Together, the realizations form one thick line, with the thickness proportional to the downscaling uncertainty.

Table 2. Bias in Seasonal Precipitation and Temperature for Both Scenarios

Season	Bias in Seasonal Precipitation		Bias in Seasonal Temperature	
	Scenario 1	Scenario 2	Scenario 1	Scenario 2
Summer (DJF)	-0.554	-0.404	-0.144	-0.044
Autumn (MAM)	-0.219	-0.140	-0.299	-0.236
Winter (JJA)	-0.882	-0.791	-0.040	-0.006
Spring (SON)	-1.034	-0.945	-0.049	-0.053

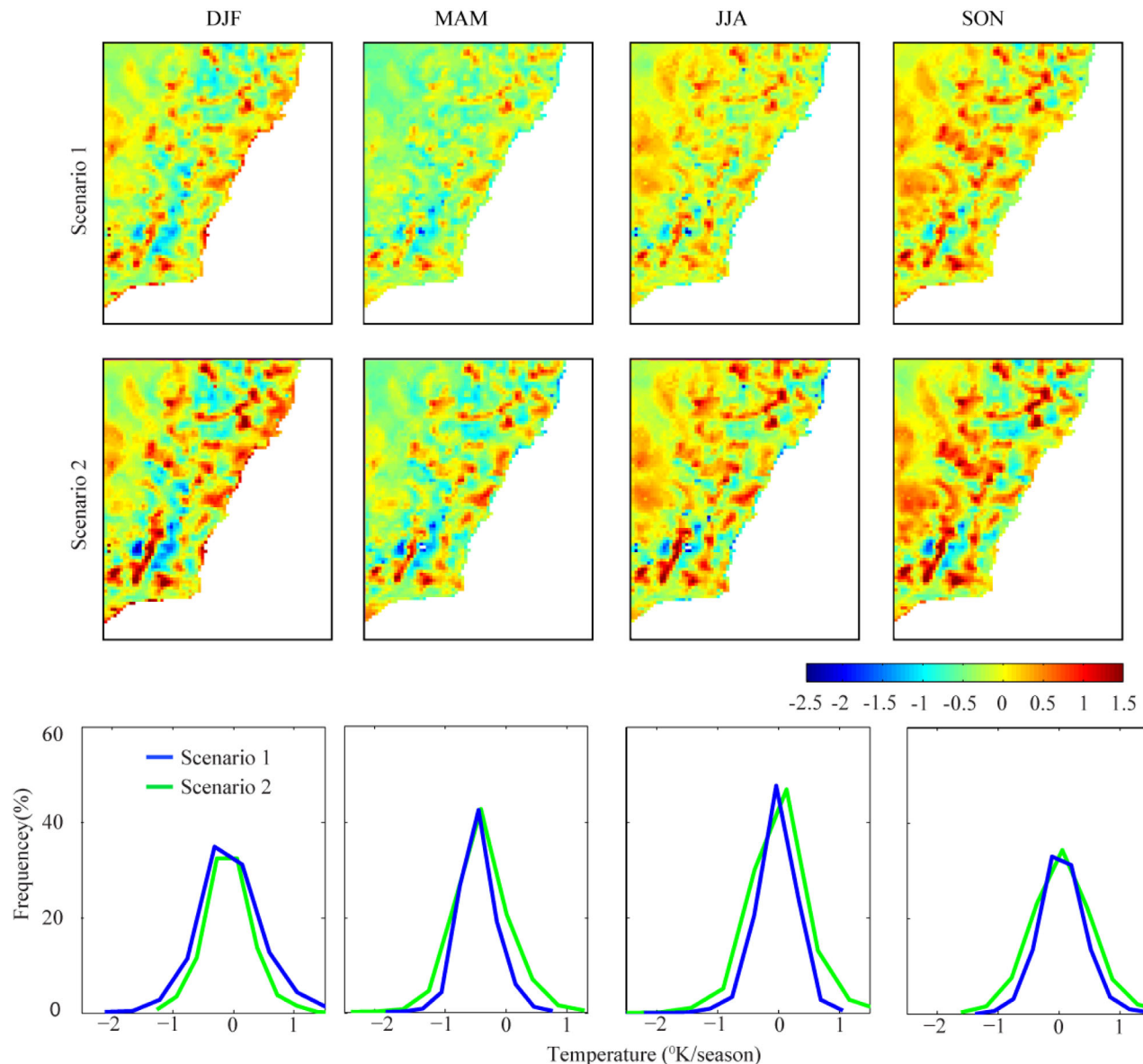


Figure 8. Comparison of seasonal mean temperature bias plots obtained for (first row) Scenario 1 and (second row) Scenario 2. (third row) Corresponding pdfs. DJF, MAM, JJA, and SON define the seasons of summer, autumn, winter, and spring respectively.

Inspection of Figure 9a indicates that the output from 25 realizations of Scenario 1 reproduces the time series pattern observed in the WRF reference. Precipitation events with small and large peaks occur on the same day as in the reference. It can be observed that the down-scaled model tends to overestimate in some cases (for example, at E2, E3, E4, E6, E7, and so on) and underestimate (for example, at E1, E5, E8, and so on) in others. In Figure 9b, analysis suggests that the temporal patterns are also well captured. In particular, the effect of including the previous day's information results in peaks that better match those of the reference. This can be seen by comparing Figure 9a and Figure 9b, where some of the marked peaks are better captured (see for example, E3, E5, E8, E11, E12, E20, E24, and E25), while the performance at other peaks is not decreased.

Similar observations can be made for Figure 10, where the time series plots for temperature are presented. By comparing Figure 10a and Figure 10b, it is clear that the range of values produced from Scenario 2 has reduced, while there are no significant changes in terms of capturing the peak values. Here the changes in MPS simulation output from Scenario 1 to Scenario 2 are clearly visible; therefore, events E1 to E30 (as used in Figure 9) are not pointed out. From a stochastic modeling perspective, this is explained by the addition of information that results in reduced uncertainty in the estimated down-scaled values.

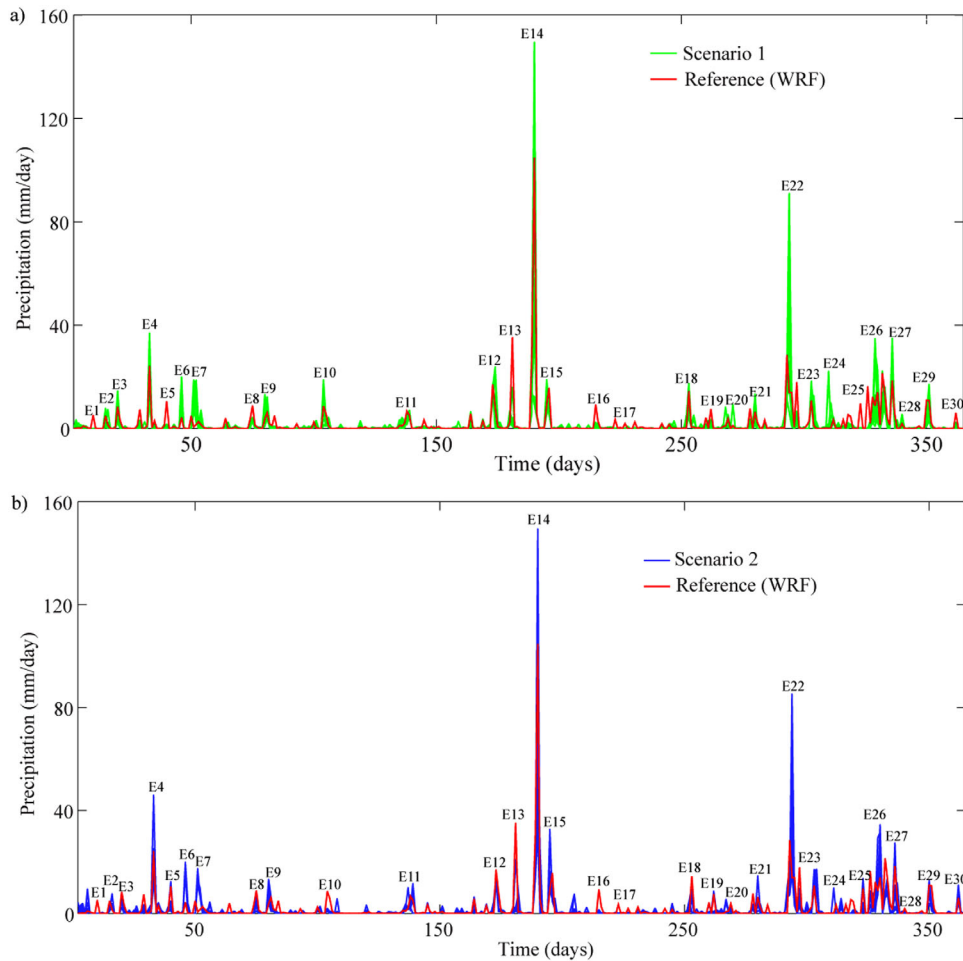


Figure 9. (a) Comparison of annual time series of precipitation at one downscaled grid pixel against the WRF reference (Scenario 1), and (b) comparison of annual time series of precipitation with the reference for Scenario 2. There are 25 green and blue lines shown in each of the plots, corresponding to the 25 downscaled realizations at each time step. E1 to E30 are marked on the plot to compare the MPS simulation results of Scenario 1 and Scenario 2 for 30 precipitation events with significant amounts of rain.

In order to evaluate the preservation of temporal continuity in a quantitative manner, we used temporal variograms. Figure 11a shows a comparison of the variogram for precipitation and temperature computed for the downscaled model and for the reference. The horizontal axis is the lag distance in time (number of days) and the vertical axis is the variogram value as a function of separation distance. It is found that globally the variograms of individual realizations are clustered around the variogram of the reference, and that the overall variogram shape is preserved in all variograms. Figure 11b presents the same variogram for temperature, with significant reduction in the spread of variograms, reflecting the fact that temperature has a more regular temporal behavior than rainfall and is therefore easier to reproduce.

The results above are only valid for a single grid pixel, and while they allow a discussion of the behavior of the downscaling approach, they are of course particular to a single location. Similar plots are required at all grid pixels (71×91) to be able to confidently derive conclusions. For that purpose, we estimate the root-mean-squared error (RMSE) between the variogram produced from results of DS simulations and the reference at each grid point. The RMSE is calculated for each realization and the mean RMSE at each pixel is represented in Figure 12. Figure 12a and Figure 12b correspond to RMSE plots for Scenarios 1 and 2, respectively.

As can be seen, in the north-east corner of Figure 12 there is a zone where the RMSE is high. This does not mean that the precipitation is poorly estimated at this location, but rather that the temporal variability, or intermittence of precipitation, is poorly reproduced. While both plots look similar, there are areas in Figure 12b where the RMSE is lower compared to Figure 12a. This is confirmed by the average values of the RMSE

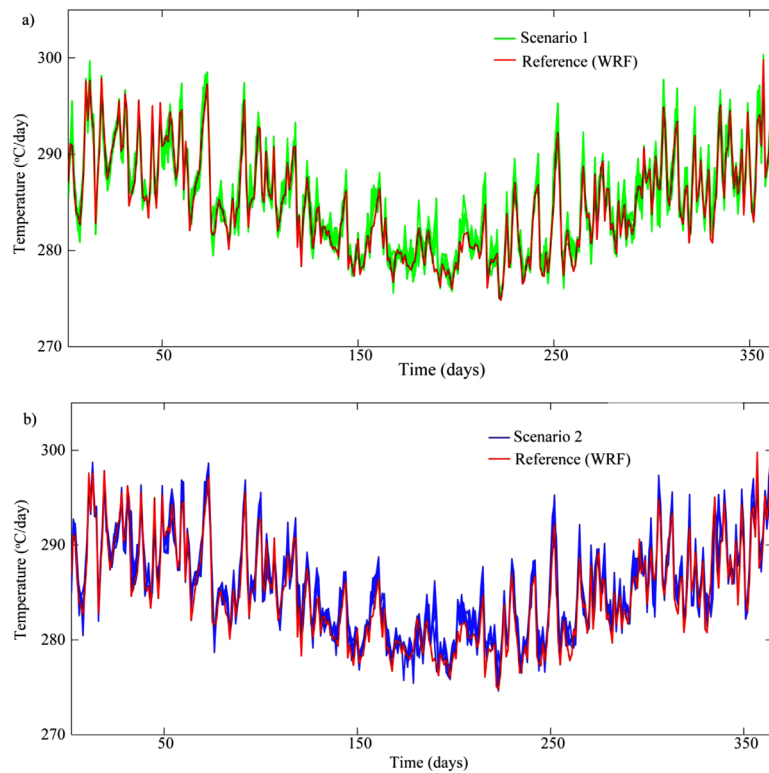


Figure 10. (a) Comparison of annual time series of temperature at one downscaled grid pixel against the WRF reference (Scenario 1), and (b) comparison of annual time series of temperature with the reference for Scenario 2 (considering time dependence). There are 25 red and blue lines shown in each of the plots, corresponding to the 25 downscaled realizations at each time step.

over the entire domain, which is 24 mm year 1 for Scenario 1 and 21 mm year 1 for Scenario 2, confirming the benefit of including temporal dependence in the downscaling procedure.

3.6. Spatiotemporal Dependence

As a final evaluation of the MPS approach, we develop an inspection procedure that considers simultaneously the reproduction of the spatial and the temporal behavior, and use it to verify whether the simulations and the reference share these properties. It consists of four steps: (i) randomly select 1000 grid nodes from the

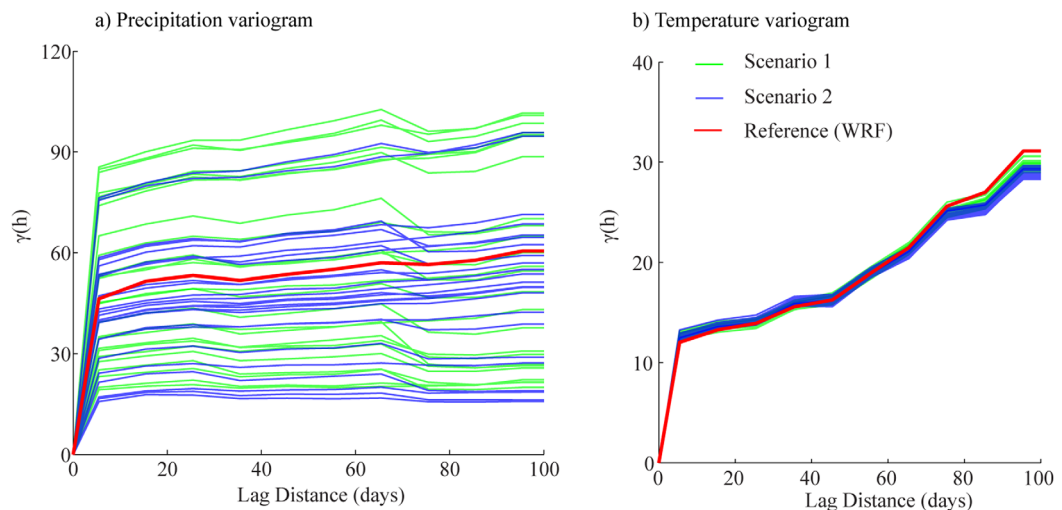


Figure 11. Comparison of variograms obtained from 25 realizations of MPS output and the reference at single grid point of time series data for (a) precipitation and (b) temperature.

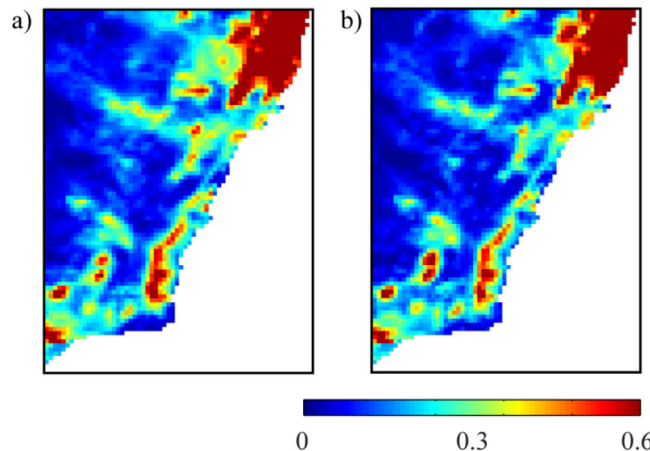


Figure 12. Plots of average root-mean-square errors (RMSE) between variograms of 25 realizations of precipitation and the reference. Results obtained from (a) Scenario 1 and (b) Scenario 2 are used.

reference data and extract the corresponding 1000 time series at these locations for the year 2005; (ii) compute the correlation coefficient between each pair of time series (in total 499,000 correlation coefficients); (iii) compute correlation coefficients using a downscaled MPS output, using the same 1000 locations for extracting time series; (iv) repeat step (iii) for all 25 realizations thus providing an ensemble of correlation coefficients; and (v) plot correlation coefficients obtained from step (ii) and (iv). This ensemble of correlation values provide a rich representation of spatiotemporal variability of the variables considered, since it takes into account both temporal dependence (because it is computed by comparing entire time series) as well as spatial dependence (time series for nearby locations are likely to be highly correlated). In a sense, this measure is in the same spirit as the computation of a variogram cloud, except that entire time series are used instead of point values.

Figure 13 compares the results of the spatiotemporal correlation coefficients for reference and realizations, for precipitation and temperature, respectively, and for Scenarios 1 and 2 individually. Each point on these plots represents a pair of locations. It is expected that nearby pairs of locations will have correlated time series, whereas location pairs further apart will have very different (uncorrelated) time series. If the cloud of points is aligned around the 1:1 line, it means that the downscaled realizations are able to reproduce the same spatiotemporal behavior as the reference, for all separation distances between points.

It can be observed that it is more challenging to accurately reproduce the behavior of precipitation (Figures 13a and 13b) than that of temperature (Figures 13c and 13d), where the cloud of points falls very close to the 1:1 line. Overall, the downscaled realizations tend to slightly overestimate the spatiotemporal dependence compared to the reference, with stronger overestimation in Scenario 2.

4. Discussion

4.1. Note on Extreme Events

The MPS downscaling method is based on the direct sampling geostatistical approach, whose underlying principle is a resampling of the training data values. Although this method has been demonstrated to correctly reproduce patterns (either spatial or temporal), it is not designed to extrapolate extreme values beyond those present in the training data. This property of direct sampling has been thoroughly investigated by *Oriani et al.*, [2014], and it is acknowledged here that the downscaled outputs of the methodology presented in this paper generally cannot be used for the type of application that involve the estimation of extreme values. The solution adopted to obtain a wide range of values is to use a very large training image, as is the case in the present study, where several years of data are used to enlarge the pool of available patterns. It results in a regionalization of the estimates that provides more robust statistics.

Such a large training image might, however, not contain extreme events with large average recurrence intervals, such as rainfall intensities with return intervals of 100 years or more. Our approach is not appropriate for such uses of precipitation data. Rather, it is designed for applications where the intermittence and

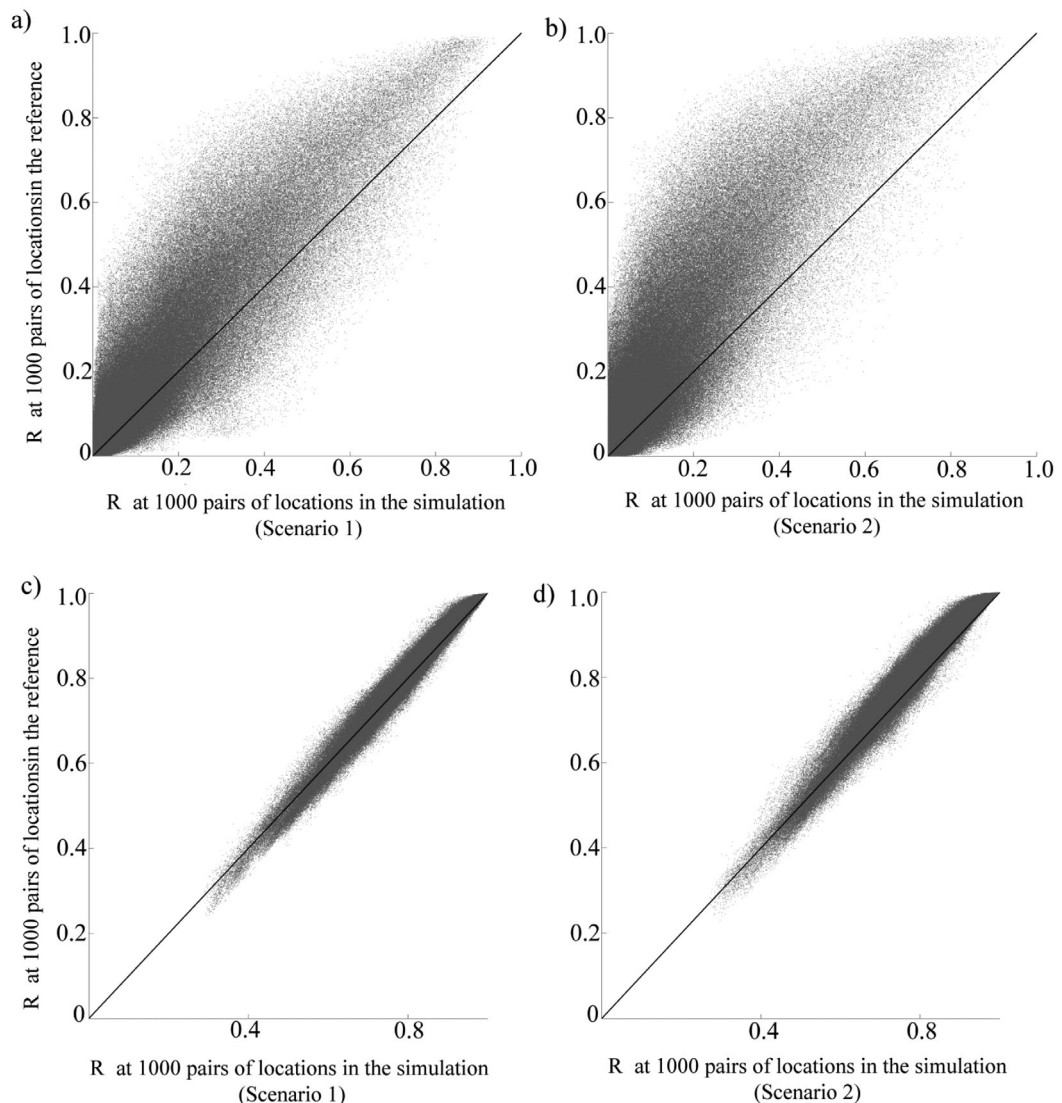


Figure 13. Comparison of spatial and temporal correlations of precipitation and temperature time series for randomly selected pairs of locations. The correlation coefficient (R) between time series of precipitation at 1000 grid nodes in the reference and in 25 downscale realizations for the precipitation of (a) Scenario 1, (b) Scenario 2 and the temperature of (c) Scenario 1 and (d) Scenario 2.

the spatial structure of rainfall are critical. For example, the occurrence of floods in large catchments is strongly related to antecedent conditions as well as to the areal extent of high rainfall values, and in those cases localized extreme precipitation values do not play a large role.

More generally, our method falls within the family of nonparametric approaches that do not model the simulated values with continuous distributions whose tail properties can be parameterized. One possibility would be to use direct sampling to downscale rainfall occurrences and in a second step, use a parametric model to draw values with one of the existing probability models that includes extreme values [Paschalis *et al.*, 2013; Schleiss *et al.*, 2014]. The potential application of such an approach will be investigated in further studies.

4.2. Alternate Sources of Training Images

The source of training image in MPS approach could be any data set which provides sufficiently long information and covers the study area. It could consist in measurements at point locations such as rain gauges or remote sensing images obtained from satellites or radar.

The available information on grids such as remote sensing images or reanalysis data can be used as long as data are available for sufficiently long duration. For example, in the present study area, radar data are

available at 5 min interval at a resolution of $1 \text{ km} \times 1 \text{ km}$, but only for 3 years duration, which is insufficient. In areas where longer radar records are available, the approach presented in this study can be adapted.

4.3. Computational Requirement

The CPU cost for running the WRF model is 6000 CPU hours to complete 1 year of simulation. The downscaling performed using MPS presented in this study takes about 100 CPU hours to produce 25 realizations that are comparable to the WRF outputs according to a range of metrics. The MPS approach has two advantages—(i) it takes several orders of magnitude less time to produce results; and (ii) it provides an ensemble which is used for uncertainty analysis, while WRF produces a single output only. Due to constraint in CPU hours, there is practically no possibility of performing uncertainty in WRF dynamical downscaling approach.

5. Conclusion

A geostatistical approach based on multiple-point statistics (MPS) was developed and applied to downscale precipitation and temperature from a 50 km grid resolution to a higher 10 km grid resolution. The MPS approach is based on training data, which can, as in our study, come from a model. Alternatively, recurrent remote sensing-based data could also be used. The proposed approach is multivariate, resulting in both precipitation and temperature being downscaled together, while maintaining their fine-scale interdependence. The approach is evaluated against WRF data for a single year immediately following the training data set. Two types of simulations are performed: a first scenario that does not consider time dependence and a second scenario that includes temporal dependence. Results indicate that the inclusion of temporal information only slightly improves the downscaling performance in both precipitation and temperature predictions. Our interpretation is that in the studied problem, the time dependence is relatively well constrained because it is conditioned to daily WRF data. In other words, the temporal variability is already very well represented in the conditioning data. This would have been different if we had performed downscaling in both space and time domains, i.e., increasing at the same time the spatial and the temporal resolution of the WRF. In this case, using a setting similar to the one of Scenario 2 would allow to introduce a temporal variability that is not originally present in the WRF outputs.

Skill score maps, bias maps, variogram analysis, and a new test for spatiotemporal characterization all converge to indicate that the downscaling procedure is able to produce complex patterns that have the same features as the 20 year training data. A general observation is that, unsurprisingly, it is much more challenging to reproduce the properties of precipitation than temperature, because rainfall is known to have an irregular or even chaotic spatiotemporal behavior. The discontinuous nature of precipitation explains why the downscaling results can present deviations when compared to the reference observations. For example, for the downscaled precipitation, a negative bias between model predictions and reference is found in all cases, indicating that the downscaled models have a tendency to underestimate the precipitation events. The bias, however, is small in magnitude, being generally much less than 1 mm d^{-1} .

Future investigations will focus on applying our downscaling approach to cases where observed data can be used for validation of the results. In this study, we used WRF output at 10 km resolution for validation which is already available, which is a favorable scenario compared to using real data. Another interesting avenue where present study can be extended is to areas where scarce or no historical data are available, which makes it difficult to develop a training image. The information from climatically similar regions will then need to be used as an analog to derive valid training data. How to select a climatically similar region and how many years of data are necessary are some of the basic questions to be explored in this topic.

Acknowledgments

This paper was supported by a postdoctoral research fellowship under the National Center for Groundwater Research and Training (NCGRT), a joint initiative between the Australian Research Council and the National Water Commission. Jason Evans and Ashish Sharma were supported by the Australian Research Council Future Fellowships FT110100576 and FT100100197, respectively. The data used in this study are available on request.

References

- Alaya, M. B., F. Chebana, and T. Ouarda (2015), Probabilistic multisite statistical downscaling for daily precipitation using a Bernoulli-generalized pareto multivariate autoregressive model, *J. Clim.*, 28, 2349–2364.
- Almazroui, M. (2012), Dynamical downscaling of rainfall and temperature over the Arabian Peninsula using RegCM4, *Clim. Res.*, 52, 49–62.
- Atkinson, P., E. Pardo-Igúzquiza, and M. Chica-Olmo (2008), Downscaling cokriging for super-resolution mapping of continua in remotely sensed images, *IEEE Trans. Geosci. Remote Sens.*, 46(2), 573–580.
- Bardossy, A., and E. J. Plate (1992), Space-time model for daily rainfall using atmospheric circulation patterns, *Water Resour. Res.*, 28(5), 1247–1259.
- Biau, G., E. Zorita, H. von Storch, and H. Wackernagel (1999), Estimation of precipitation by kriging in the EOF space of the sea level pressure field, *J. Clim.*, 12(4), 1070–1085.

- Boucher, A., P. C. Kyriakidis, and C. Cronkite-Ratcliff (2008), Geostatistical solutions for super-resolution land cover mapping, *IEEE Trans. Geosci. Remote Sens.*, 46(1), 272–283.
- Caers, J., and T. Zhang (2005), Multiple-point geostatistics: A quantitative vehicle for integrating geologic analogs into multiple reservoir models, *AAPG Memoir*, (80), 383–394.
- Comunian, A., S. Jha, B. Giambastiani, G. Mariethoz, and B. Kelly (2014), Training images from process-imitating methods, *Math. Geosci.*, 46(2), 241–260, doi:10.1007/s11004-013-9505-y.
- Dai, A., W. Washington, G. Meehl, T. Bettge, and W. Strand (2004), The ACPI climate change simulations, *Clim. Change*, 62(1–3), 29–43.
- Emery, X., and C. Lantuéjoul (2014), Can a training image be a substitute for a random field model?, *Math. Geosci.*, 46(2), 133–147, doi:10.1007/s11004-013-9492-z.
- Evans, J. P., and M. F. McCabe (2010), Regional climate simulation over Australia's Murray-Darling basin: A multitemporal assessment, *J. Geophys. Res.*, 115, D14114, doi:10.1029/2010JD013816.
- Fiorucci, P., P. La Barbera, L. Lanza, and R. Minciardi (2001), A geostatistical approach to multisensor rain field reconstruction and downscaling, *Hydrol. Earth Syst. Sci. Discuss.*, 5(2), 201–213.
- Fowler, H., S. Blenkinsop, and C. Tebaldi (2007), Linking climate change modelling to impacts studies: Recent advances in downscaling techniques for hydrological modelling, *Int. J. Climatol.*, 27(12), 1547–1578.
- Ge, Y., and H. Bai (2010), MPS-based information extraction method for remotely sensed imagery: A comparison of fusion methods, *Can. J. Remote Sens.*, 36(6), 763–779.
- Ge, Y., and H. Bai (2011), Multiple-point simulation-based method for extraction of objects with spatial structure from remotely sensed imagery, *Int. J. Remote Sens.*, 32(8), 2311–2335.
- Honarkhah, M., and J. Caers (2012), Direct pattern-based simulation of non-stationary geostatistical models, *Math. Geosci.*, 44(6), 651–672.
- Iorio, J., P. Duffy, B. Govindasamy, S. Thompson, M. Khairoutdinov, and D. Randall (2004), Effects of model resolution and subgrid-scale physics on the simulation of precipitation in the continental United States, *Clim. Dyn.*, 23(3–4), 243–258.
- Jha, S. K., G. Mariethoz, and B. Kelly (2013a), Bathymetry fusion using multiple-point geostatistics: Novelty and challenges in representing non-stationary bedforms, *Environ. Modell. Software*, 50, 66–76, doi:10.1016/j.envsoft.2013.09.001.
- Jha, S. K., G. Mariethoz, J. P. Evans, and M. F. McCabe (2013b), Demonstration of a geostatistical approach to physically consistent downscaling of climate modeling simulations, *Water Resour. Res.*, 49, 245–259, doi:10.1029/2012WR012602.
- Jha, S. K., A. Comunian, G. Mariethoz, and B. Kelly (2014), Parameterization of training images for aquifer 3D facies modeling integrating geological interpretations and statistical inference, *Water Resour. Res.*, 50, 7731–7749, doi:10.1002/2013WR014949.
- Jiang, X., and Z.-L. Yang (2012), Projected changes of temperature and precipitation in Texas from downscaled global climate models, *Clim. Res.*, 53, 229–244.
- Journel, A., and T. Zhang (2006), The necessity of a multiple-point prior model, *Math. Geol.*, 38(5), 591–610.
- Lanza, L., J. Ramírez, and E. Todini (2001), Stochastic rainfall interpolation and downscaling, *Hydrol. Earth Syst. Sci. Discuss.*, 5(2), 139–143.
- Maraun, D., et al. (2010), Precipitation downscaling under climate change: Recent developments to bridge the gap between dynamical models and the end user, *Rev. Geophys.*, 48, RG3003, doi:10.1029/2009RG000314.
- Mariethoz, G., P. Renard, and J. Straubhaar (2010), The Direct Sampling method to perform multiple-point geostatistical simulations, *Water Resour. Res.*, 46, W11536, doi:10.1029/2008WR007621.
- Mariethoz, G., M. F. McCabe, and P. Renard (2012), Spatio-temporal reconstruction of gaps in multivariate fields using the Direct Sampling approach, *Water Resour. Res.*, 48, W10507, doi:10.1029/2012WR012115.
- McGregor, J. (1997), Regional climate modelling, *Meteorol. Atmos. Phys.*, 63(1), 105–117.
- Meerschman, E., G. Pirot, G. Mariethoz, J. Straubhaar, M. Van Meirvenne, and P. Renard (2013), A practical guide to performing multiple-point statistical simulations with the direct sampling algorithm, *Comput. Geosci.*, 52, 307–324.
- Mehrotra, R., and A. Sharma (2007), Preserving low-frequency variability in generated daily rainfall sequences, *J. Hydrol.*, 345(1), 102–120.
- Meng, X., J. Evans, and M. McCabe (2014), The impact of observed vegetation changes on land–atmosphere feedbacks during drought, *J. Hydrometeorol.*, 15(2), 759–776.
- Neuweiler, I., A. Papafotiou, H. Class, and R. Helmig (2011), Estimation of effective parameters for a two-phase flow problem in non-Gaussian heterogeneous porous media, *J. Contam. Hydrol.*, 120–121(C), 141–156.
- Oriani, F., J. Straubhaar, P. Renard, and G. Mariethoz (2014), Simulation of rainfall time series from different climatic regions using the direct sampling technique, *Hydrol. Earth Syst. Sci.*, 18(8), 3015–3031.
- Paschalidis, A., P. Molnar, S. Fatichi, and P. Burlando (2013), A stochastic model for high-resolution space-time precipitation simulation, *Water Resour. Res.*, 49, 8400–8417, doi:10.1002/2013WR014437.
- Perkins, S., A. Pitman, N. Holbrook, and J. McAneney (2007), Evaluation of the AR4 climate models' simulated daily maximum temperature, minimum temperature, and precipitation over Australia using probability density functions, *J. Clim.*, 20(17), 4356–4376.
- Schleiss, M., S. Chamoun, and A. Berne (2014), Stochastic simulation of intermittent rainfall using the concept of "dry drift", *Water Resour. Res.*, 50, 2329–2349, doi:10.1002/2013WR014641.
- Strebelle, S. (2002), Conditional simulation of complex geological structures using multiple-point statistics, *Math. Geol.*, 24(1), 1–22.
- Sun, L., H. Li, S. E. Zebiak, D. F. Moncunill, F. D. Filho, and A. D. Moura (2006), An operational dynamical downscaling prediction system for Northeast Brazil and the 2002–04 real-time forecast evaluation, *J. Clim.*, 19(10), 1990–2007.
- Tang, Y., P. M. Atkinson, and J. Zhang (2015), Downscaling remotely sensed imagery using area-to-point cokriging and multiple-point geostatistical simulation, *ISPRS J. Photogramm. Remote Sens.*, 101, 174–185.
- von Storch, H. (1999), On the use of "inflation" in statistical downscaling, *J. Clim.*, 12(12), 3505–3506.
- Vrac, M., and P. Naveau (2007), Stochastic downscaling of precipitation: From dry events to heavy rainfalls, *Water Resour. Res.*, 43, W07402, doi:10.1029/2006WR005308.
- Wojcik, R., D. McLaughlin, A. G. Konings, and D. Entekhabi (2009), Conditioning stochastic rainfall replicates on remote sensing data, *IEEE Trans. Geosci. Remote Sens.*, 47(8), 2436–2449.
- Zhang, X., H. Jiang, G. Zhou, Z. Xiao, and Z. Zhang (2012), Geostatistical interpolation of missing data and downscaling of spatial resolution for remotely sensed atmospheric methane column concentrations, *Int. J. Remote Sens.*, 33(1), 120–134.
- Zinn, B., and C. Harvey (2003), When good statistical models of aquifer heterogeneity go bad: A comparison of flow, dispersion, and mass transfer in connected and multivariate Gaussian hydraulic conductivity fields, *Water Resour. Res.*, 39(3), 1051, doi:10.1029/2001WR001146.